

Ferredoxin5 Deletion Affects Metabolism of Algae during the Different Phases of Sulfur Deprivation¹

Venkataramanan Subramanian,^{a,2} Matt S.A. Wecker,^{a,b} Alida Gerritsen,^a Marko Boehm,^{a,3} Wei Xiong,^a Benton Wachter,^a Alexandra Dubini,^{a,4} David González-Ballester,^d Regina V. Antonio,^c and Maria L. Ghirardi^{a,5,6}

^aBiosciences Center, National Renewable Energy Laboratory, Golden, Colorado 80401

^bGeneBiologics, LLC, Boulder, Colorado 80303

^cUniversity Federal de Santa Catarina, Florianopolis, 476 Santa Catarina, Brazil

^dUniversity of Córdoba, 14071 Córdoba, Spain.

ORCID IDs: 0000-0001-5656-9528 (V.S.); 0000-0003-1877-9908 (M.S.A.W.); 0000-0003-3148-8427 (A.G.); 0000-0003-4049-0174 (M.B.); 0000-0003-0492-0296 (B.W.); 0000-0001-8825-3915 (A.D.); 0000-0003-0024-1886 (D.G.-B.); 0000-0003-0369-1997 (R.V.A.); 0000-0002-0885-6044 (M.L.G.).

Ferredoxin5 (FDX5), a minor ferredoxin protein in the alga *Chlamydomonas* (*Chlamydomonas reinhardtii*), helps maintain thylakoid membrane integrity in the dark. Sulfur (S) deprivation has been used to achieve prolonged hydrogen production in green algae. Here, we propose that FDX5 is involved in algal responses to S-deprivation as well as to the dark. Specifically, we tested the role of FDX5 in both the initial aerobic and subsequent anaerobic phases of S-deprivation. Under S-deprived conditions, absence of FDX5 causes a distinct delay in achieving anoxia by affecting photosynthetic O₂ evolution, accompanied by reduced acetate uptake, lower starch accumulation, and delayed/lower fermentative metabolite production, including photohydrogen. We attribute these differences to transcriptional and/or posttranslational regulation of acetyl-CoA synthetase and ADP-Glc pyrophosphorylase, and increased stability of the PSII D1 protein. Interestingly, increased levels of FDX2 and FDX1 were observed in the mutant under oxic, S-replete conditions, strengthening our previously proposed hypothesis that other ferredoxins compensate in response to a lack of FDX5. Taken together, the results of our omics and pull-down experiments confirmed biochemical and physiological results, suggesting that FDX5 may have other effects on *Chlamydomonas* metabolism through its interaction with multiple redox partners.

Ferredoxins are small iron sulfur (S)-containing proteins that distribute reductant from fermentative and photosynthetic donors to various metabolic pathways, such as carbon fixation, nitrogen assimilation, sulfite reduction, and H₂ production. The genome of the green alga *Chlamydomonas reinhardtii* (hereafter *Chlamydomonas*) revealed the presence of 13 putative ferredoxin homologs (Yang et al., 2015). The specific role of these homologs is not known, although it has been shown that the major ferredoxin1 (FDX1) performs NADP⁺ reduction in vivo, displays high transcript levels in cultures grown under photoautotrophic or photoheterotrophic conditions (Terauchi et al., 2009), and has the ability to reduce NADP⁺ in vitro upon addition of light-activated PSI and ferredoxin-NADP oxidoreductase (Yacoby et al., 2011; Boehm et al., 2016). Interestingly, these two in vitro reactions are also mediated by one of the other minor ferredoxins, FDX2, but not by FDX3, 4, or 5 (Boehm et al., 2016).

Terauchi et al. (2009) performed an initial assignment of six ferredoxin homologs to specific pathways based on their intracellular location and predominance of their transcripts or protein products under multiple stress conditions. Their studies showed that FDX5 is present in the chloroplast fraction and its expression is induced under dark hypoxic conditions. Moreover,

previous work demonstrated that FDX5 transcripts are also up-regulated during the hypoxic and anaerobic phases of S-deprivation (Jacobs et al., 2009; Lambertz et al., 2010), and even under oxic, S-deprived conditions (Zalutskaya et al., 2018).

Previously, we carried out a detailed analysis of ferredoxin protein interactors using heterologously expressed individual ferredoxins (1, 2, 3, 4, and 5) as baits, and identified potential interactors with each of them. Those results yielded several clues as to the possible physiological role of each homolog (Peden et al., 2013). Furthermore, we also observed that redox potentials of all the five ferredoxins, based on in vitro assays, are more positive (~-320 mV) in comparison to that of FDX1 (-420 mV; Boehm et al., 2016; M. Boehm, E. Peden, and A. Dubini, unpublished data). Taken together, these results suggested possible interactions between FDX5 and other proteins such as mitogen activated protein kinase (MAPK6), starch branching enzyme (SBE3), desaturase (DES6), peroxiredoxin (PRX1), cell wall glycoprotein, and hydrogenase maturation protein (HYDEF; Peden et al., 2013). This information served as a guide in this work for further exploration of the role of FDX5 in *Chlamydomonas* redox metabolism under a specific stress condition, S-deprivation, known to induce its expression.

A few years ago, the Grossman laboratory generated a *FDX5* knock-out mutant and described a dark phenotype, under S-replete conditions, that was caused by the lack of fatty acid desaturation activity (Yang et al., 2015), and which resulted in a major disruption of the cell membrane of the mutant, thus confirming our initial assignment of the DES6 desaturase as interactor with *FDX5* (Peden et al., 2013). In this work we further characterized the phenotype of the *FDX5* knock-out mutant under S-deprivation, a well-studied stress condition that induces H₂ production, and that is composed of an initial aerobic and a subsequent anaerobic phase. It is important to keep in mind that S-deprivation induces expression not only of anaerobically regulated genes but also of those involved in S-stress response, particularly during the initial aerobic phase (González-Ballester et al., 2010). Additionally, we performed an omics-based assessment of the involvement of *FDX5* in some of the other pathways in which it has been suggested to have a role based on previous studies, such as aerobic starch accumulation, anaerobic fermentative metabolism, and hydrogenase biosynthesis (Peden et al., 2013).

Our results indicate that the phenotype of the S-deprived *fdx5* strain differs from that of the wild type under both the aerobic and anaerobic phases, and that it is also different in many respects from that described by Yang et al. (2015) under dark incubation. We show that deletion of *FDX5* leads to a distinctive delay in the

organism's physiological response to S stress and also confirms *FDX5*'s interaction with various previously identified pathways. Finally, our work provides initial evidence for the compensatory effect that other ferredoxins may play when one of them (in this case, *FDX5*) is knocked out.

RESULTS

One of the characteristics of wild-type CC-124 *Chlamydomonas* is its response to S-deprivation, whereby cultures undergo gradual anaerobiosis and subsequent H₂ photoproduction (Melis et al., 2000; Kosourov et al., 2002). Given the previously described inability of *fdx5* to grow in the dark (Yang et al., 2015), a condition that favors anaerobiosis, we used a different *fdx5*-inducing condition, S-deprivation, to assess the mutant's response to anoxia in the light to identify additional *fdx5* phenotypes.

Lower Oxygen Evolution and Respiration Rates in *fdx5* under Sulfur-Deprivation Conditions

The effects of *FDX5* deletion on respiratory and photosynthetic capacity were measured under S-replete conditions and increasing light intensities in the presence of added bicarbonate (Kosourov et al., 2002). As shown in Table 1, there were no significant differences between the wild type and mutant under any tested light intensities (except perhaps at 2,000 $\mu\text{E m}^{-2} \text{s}^{-1}$), reflecting the lack of influence of *FDX5* on these reactions, in agreement with Yang et al. (2015). We repeated the measurements under S-depleted conditions and 100 $\mu\text{E m}^{-2} \text{s}^{-1}$ (the light intensity used for subsequent experiments) and 500 $\mu\text{E m}^{-2} \text{s}^{-1}$ (saturating light) illumination at 24 and 48 h after the start of S-deprivation process. Table 1 also shows that net O₂ evolution rates (i.e. measured rates of O₂ evolution corrected for O₂ consumption after turning off the light) of *fdx5* decreased more slowly than those in the wild type during the 48-h period, suggesting a longer oxygenic period under S-deprivation. Similar observations were obtained under 500 $\mu\text{E m}^{-2} \text{s}^{-1}$, confirming a slower response of *fdx5* to S-deprivation in inactivating net O₂ evolution.

Chlorophyll Levels and Headspace Gas Composition of *fdx5* in Comparison to Wild Type under Sulfur Deprivation

Cultures were transferred into -S medium and monitored for chlorophyll concentration and gas levels in the headspace during the initial aerobic period and the subsequent anaerobic phase.

Chlorophyll content increased in both strains during the first 24 h of S-deprivation (Fig. 1A), followed by a gradual decrease until 120 h, as previously reported for the wild type (Kosourov et al., 2002). During this time

¹This work was supported in part by the National Renewable Energy Laboratory, operated by the Alliance for Sustainable Energy LLC, for the United States Department of Energy (DOE, contract no DE-AC36-08GO28308), the Department of Energy's Office of Science, Biological and Environmental Research (M.L.G.), the European Research Area Net for the Mediterranean area program (ERANETMED2-72-300 to D.G.-B.), the Talent Hub program (291780 to A.D.), and the Brazilian Foundation Coordenação de Aperfeiçoamento de Pessoal de Nível Superior (CAPES post-doctoral fellowship to R.V.A.).

²Author for contact: venkat.subramanian@nrel.gov.

³Present address: Botanical Institute, Christian-Albrechts-University, 24118 Kiel, Germany.

⁴Present address: University of Córdoba, 14071 Córdoba, Spain.

⁵Retired

⁶Senior author.

The author responsible for distribution of materials integral to the findings presented in this article in accordance with the policy described in the Instructions for Authors (www.plantphysiol.org) is: Venkataraman Subramanian (venkat.subramanian@nrel.gov).

V.S. and M.L.G. wrote the article and supervised the project; V.S., M.S.A.W., A.D., and M.L.G. designed the experiments; V.S., M.S.A.W., R.V.A., B.W., A.D., and D.G.-B. carried out molecular and physiological experiments; V.S. carried out the microscopy work; M.S.A.W. executed Clark electrode assays and reverse transcription PCR, and contributed to growing the strains under sulfur-starvation conditions; M.B. performed the pull-down assays; A.G. analyzed the transcriptomics data and created the figures; W.X. carried out the HPLC analysis; all authors participated in reviewing and editing the article.

www.plantphysiol.org/cgi/doi/10.1104/pp.19.00457

Table 1. Rates of dark O₂ consumption and photosynthetic O₂ evolution in sulfur-replete (0 h) and sulfur-deplete (24-h and 48-h) cultures under different light intensities.

Experiments were done in biological triplicates, except where indicated.

Strain	Hours under S-Deprivation	Light Intensity ($\mu\text{E. m}^{-2} \text{ s}^{-1} \text{ PAR}$)	Dark O ₂ Consumption Rate ($\mu\text{mol.mg}^{-1} \text{ chl.h}^{-1}$)	Net Photosynthetic O ₂ Evolution Rate ^a ($\mu\text{mol.mg}^{-1} \text{ chl.h}^{-1}$)
CC-124	0	50	47.4 ± 1.1	51.9 ± 3.3
		100	55.6 ± 4.0	89.7 ± 3.3
		200	59.1 ± 3.5	139.9 ± 6.0
		500	63.7 ± 2.0	212.0 ± 11.3
		1,000	68.0 ± 5.5	212.4 ± 15.2
		2,000	48.3 ± 1.6	170.9 ± 9.4
	24	100	47.6 ± 0.8	44.6 ± 3.4
		500	50.8 ± 1.2	50.0 ± 1.2
		500	15.9 ± 0.7	21.3 ± 0.9
	48	100	19.2 ± 5.0	23.9 ± 4.4
		500	15.9 ± 0.7	21.3 ± 0.9
		500	46.9 ± 3.8	57.1 ± 3.7
<i>fdx5</i>	0	50	46.9 ± 3.8	57.1 ± 3.7
		100	51.3 ± 1.1	90.0 ± 2.9
		200	56.1 ± 0.3	144.1 ± 3.6
		500	59.5 ± 3.5	198.6 ± 5.3
		1,000	60.1 ± 4.4	211.0 ± 1.5
		2,000	44.7 ± 2.0	151.3 ± 11.7
	24	100	52.5 ± 6.0	59.6 ± 5.9
		500	53.7 ± 0.7	87.9 ± 3.7
		100	33.0 (two samples)	38.5 ± 2.4
	48	100	33.0 (two samples)	38.5 ± 2.4
		500	33.4 ± 6.5	33.7 ± 10.5

^aNet photosynthetic O₂ evolution rate is calculated as measured O₂ evolution rate minus measured O₂ consumption rate.

course, chlorophyll levels of *fdx5* consistently remained lower than the wild type. At the end of 120 h, both strains showed approximately the same chlorophyll levels, which was close to the starting value at 0 h (i.e. 20 $\mu\text{g}/\text{mL}$). The results show that *fdx5* is amenable to S-deprivation and responds in a similar manner to wild type in terms of culture growth.

After a period of decreasing O₂ evolution activity, S-deprivation leads to culture anaerobiosis in wild-type strains (Kosourov et al., 2002; Zalutskaya et al., 2018), occurring at ~48 h after the start of the process in CC-124 in this study (Fig. 1B). Decreases in O₂ concentration in the reactor post S-deprivation based on total headspace analysis were slower in *fdx5* in comparison

to wild type, and full anaerobiosis was achieved later in the mutant, between 72 and 96 h in this experiment. Thus, we observed a prolongation of the aerobic phase and a delay in the establishment of anaerobiosis in *fdx5*. This observation is consistent with the higher net O₂ evolution rate in *fdx5* at 24 h post S-deprivation (Table 1), resulting in higher O₂ content in the photobioreactor at this timepoint (Fig. 1B). Accordingly, we observed that H₂ production in the wild-type strain was first detected at 48 h of S starvation, while the start of H₂ production in the mutant was delayed and initially observed only after 72 h of S-deprivation. At the end of this experiment, *fdx5* accumulated ~50% lower H₂ amounts compared to the wild type.

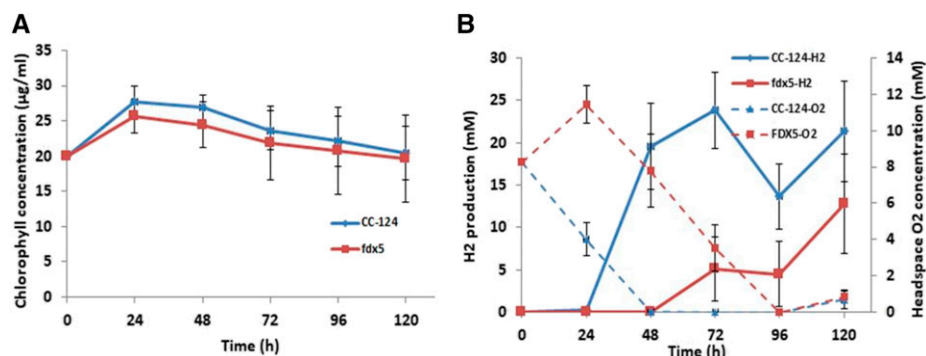


Figure 1. Chlorophyll content and headspace gas measurements. Triplicate cultures of *fdx5* (red curves) and CC-124 (blue curves) cells were grown in TAP+S media ($t = 0$) and then transferred to S-deprived media and incubated in the light for 120 h. A, Chlorophyll measurements at 24-h intervals. B, Headspace H₂ (solid blue line for CC-124 and solid red line for *fdx5*) and O₂ measurements (dashed blue line for CC-124 and dashed red line for *fdx5*) at 24-h intervals. Experiments were carried out in biological triplicates. Data are shown as mean ± sd.

Cell Integrity Assessment

We used bright-field microscopy to determine the structural integrity of the cells during the S-deprived oxic and anoxic phases. We observed that the size of *fdx5* cells seemed larger on average, under the same magnification, when compared to wild-type cells, even before the start of S-deprivation ($t = 0$, Fig. 2). Furthermore, we also observed that *fdx5* cells seemed healthier in terms of their cell shape at 120 h in comparison to wild type, whose cells appeared to lose integrity at this time point. Overall, *fdx5* cells appeared sturdier than wild type at later time points during the S-deprivation experiment, suggesting higher viability.

Lower Fermentative Metabolite Levels in *fdx5* under Sulfur-Deprived Condition

The levels of other secreted fermentative metabolites, whose accumulation is known to accompany H_2 photoproduction during the anaerobic phase of

S-deprivation (Kosourov et al., 2003; Ghirardi et al., 2018), were measured by high performance liquid chromatography (HPLC). We observed a delay in their accumulation in the mutant strain (Fig. 3), mirroring the effect on H_2 photoproduction. Formate and ethanol levels increased in both strains, although earlier and to significantly higher levels in the wild type. Levels of CO_2 , which are the combined result of respiratory and fermentative activities, also increased more quickly in the wild type. Overall these data are suggestive of higher contribution of fermentative over respiratory activity in the wild-type strain during the process. Acetate consumption, which occurs only under aerobic conditions, was observed at 24 h in both strains, although at significantly higher rates in wild type in comparison to *fdx5*. Although net acetate levels in CC-124 remained almost constant for the rest of the time period, *fdx5* showed a gradual but continued consumption of acetate, demonstrating statistically higher acetate consumption levels post 48-h S-starvation.

To better explain the slower rates of acetate utilization in *fdx5*, which is the primary C source under the aerobic phase of S-deprivation (Melis et al., 2000; Tsygankov et al., 2002; Kosourov et al., 2003), we carried out immunoblotting analysis to determine the levels of the acetate-utilizing enzyme acetyl-CoA synthetase (ACS) at the different time points (Fig. 4). We observed that the levels of ACS were comparable between the two strains up to $t = 4$. However, starting from $t = 6$, there were visible differences in its levels, with wild type showing ~2-fold higher levels of ACS compared to *fdx5*. Subsequently, ACS levels dropped in both strains at $t = 24$ and $t = 48$, although still present at detectable levels only in wild type at both these later time points. This observation suggested an association between slower rate of acetate consumption in *fdx5* with the low ACS enzyme levels in the mutant strain during the initial aerobic 48 h. In addition to ACS, we also tested the levels of fermentative pathway proteins such as the alcohol dehydrogenase (ADH1) and pyruvate-ferredoxin oxidoreductase (PFOR; Magneschi et al., 2012) that result in the generation of alcohol and CO_2 , respectively. We observed that ADH1 levels gradually increased in both strains up to $t = 6$, while peaking in wild type at $t = 24$ and in *fdx5* at 48 h, the times at which anaerobiosis was established in each culture in this experiment. This was consistent with the higher initial synthesis of ethanol, which reached higher levels by $t = 48$ in wild type, in comparison to *fdx5*. PFOR was barely detectable in either strains until $t = 24$, while being detectable only in wild type at $t = 48$. Finally, we also tested the levels of the oxygen-evolving protein D1 (encoded by *psbA*) by immunoblotting (Fig. 4). We observed that although its levels remained high in both the strains up to 6 h of S-deprivation, they decreased faster in wild type at later timepoints such that they were 2-fold lower in wild type than in *fdx5* at $t = 24$, while almost being undetectable at $t = 48$ in wild type alone. These measurements provide additional evidence of slower

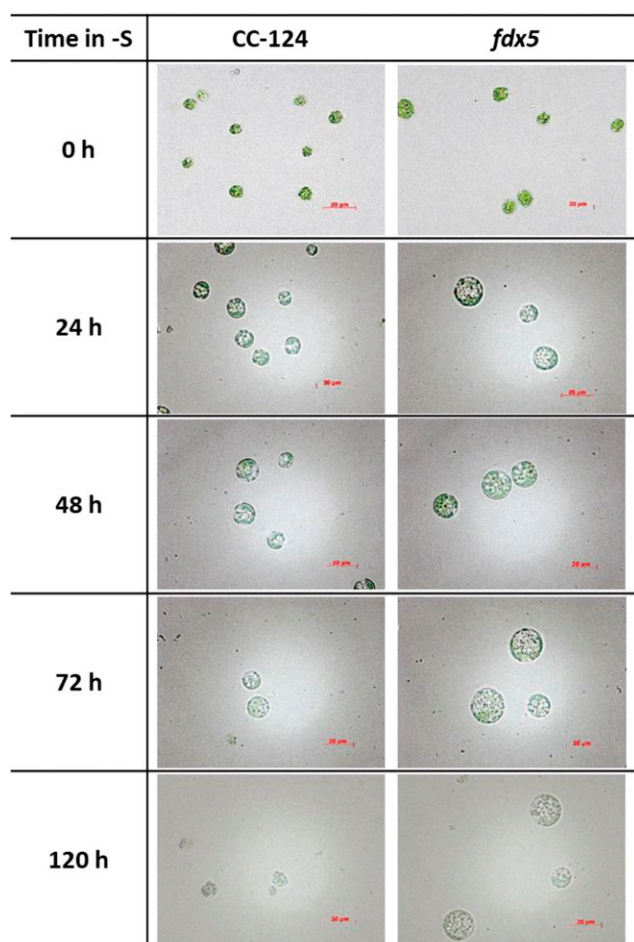
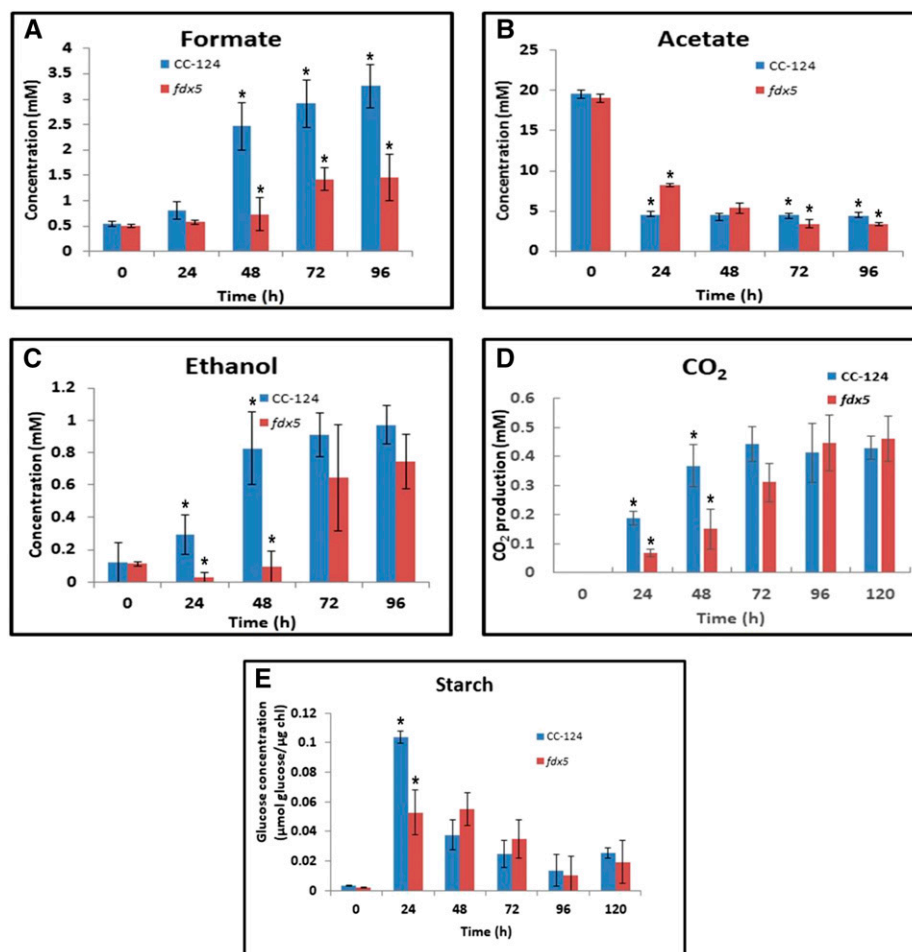


Figure 2. Cell morphology assessment. Cells were visualized at 24-h time intervals during S-deprivation (–S) with 63 \times magnification using an Axio Scope A1 microscope (Carl Zeiss). Scale bar = 20 μ m.

Figure 3. Fermentative metabolites and starch content. A to C, Measurements of formate (A), acetate (B), and ethanol (C) levels at 24-h intervals after S-deprivation were done by HPLC. D, CO₂ measurements were performed by GC. Results were obtained from three independent *fdx5* (red bars) and CC-124 (blue bars) cultures. E, Starch was assayed as the total amount of Glc released from accumulated starch upon treatment of *fdx5* (red bars) and CC-124 (blue bars) cells with amyloglucosidase enzyme. Starch results were obtained from three biological and two technical replicates collected at 24-h intervals. Data were analyzed using two-tailed Student's *t* test. Asterisks represent *P* values < 0.05. Data are shown as mean ± SD.



inactivation of PSII reaction center in the mutant strain and its longer oxygenic metabolism, as well as supporting the delayed start of anaerobiosis.

Decreased Starch Accumulation in the Mutant Strain under Sulfur-Deprived Conditions

Besides water oxidation, the other major source of reductant and carbon during the anaerobic phase of S-deprivation in *Chlamydomonas* is starch degradation. Starch levels in both strains when harvested from S-replete culture conditions were extremely low, on the order of 0.002 and 0.003 μmol Glc/μg Chl in wild type and *fdx5*, respectively (Fig. 3). As previously shown for CC-124 (Kosourov et al., 2003), maximum starch levels were reached during the aerobic phase at 24 h of S-deprivation, which corresponds to a 51-fold increase over *t* = 0. In the *fdx5* mutant, on the other hand, maximum starch levels were attained at 24 h, although remaining the same at 48 h. This increase, however, represented only a 25-fold value compared to *t* = 0. After an initial accumulation during the aerobic phase, both strains consumed starch during the anaerobic phase. Interestingly, while both wild type and the

mutant strain expressed the small subunit of AGPase STA6 to higher levels in the aerobic phase of growth (*t* = 0), its level was reduced several folds post 6 h of S-deprivation in both strains (Fig. 4). Specifically, at *t* = 24, the levels remained slightly higher in wild type and were almost undetectable at *t* = 48. On the other hand, *fdx5* showed lower levels at *t* = 24, in comparison to wild type, while maintaining detectable levels at *t* = 48 (Fig. 4), suggesting more sustained starch accumulation in the mutant strain at these later times.

Differential Expression of Ferredoxin Transcript and Proteins in *fdx5*

We had proposed previously that minor ferredoxins could perhaps perform each other's functions under specific growth conditions (Peden et al., 2013). RNA sequencing (RNA-Seq) analysis of wild-type and *fdx5* samples, collected at *t* = 0, 24, 48, and 72 h after S-deprivation, was carried out to test this hypothesis. We maintained a cut-off of ≥2-logfold to designate a gene being up- or down-regulated (Fig. 5). Most of the ferredoxin transcripts in *fdx5* were present within the cutoff limit with respect to wild type at *t* = 0 (Fig. 5A).

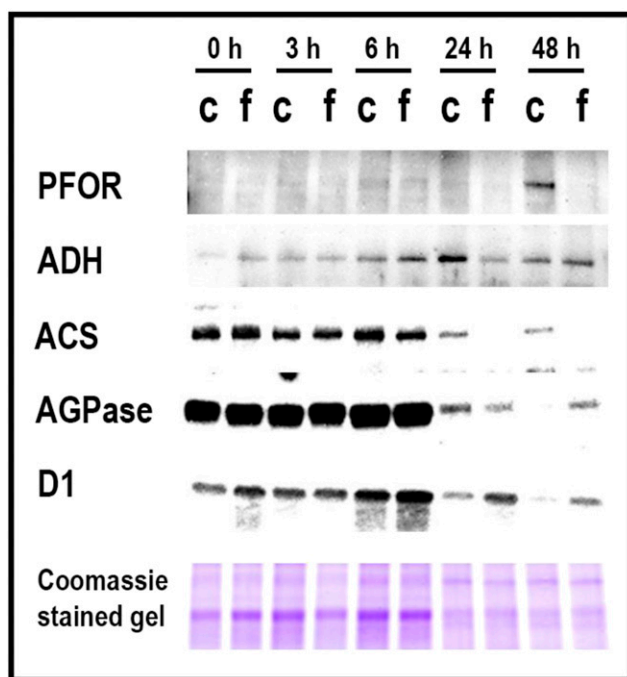


Figure 4. Expression levels of proteins involved in specific phenotypes observed during S-deprivation. Immunoblot analysis was carried out on protein extracts generated from cells harvested at $t = 0, 3, 6, 24,$ and 48 h of S-deprivation. AGPase, ADP Glc pyrophosphorylase; c, CC-124; D1, PSII reaction center protein; f, *fdx5*.

While *FDX1* transcript levels declined from $t = 0$ during the course of the S-deprivation in both strains, their down-regulation was much higher in wild type in comparison to *fdx5* (Fig. 5, B and C). *FDX2* transcripts, however, were lower in *fdx5* in comparison to wild type at $t = 0$ (Fig. 5A), while subsequently regaining wild-type levels (Fig. 5, B and C). The only other *FDX* transcript to significantly change was *FDX12*, which in the mutant was within the cutoff limit at $t = 0$ (Fig. 5A) and showed lower levels than wild type under S-deprivation conditions (Fig. 5, B and C). The function of *FDX12* is yet to be determined. *FDX5* transcript was detectable to a very low level in the *fdx5* strain in both +S and -S conditions (Fig. 5, A–C), which could be attributed to the presence of partial transcripts in the RNA-Seq technique. We confirmed expression of *FDX5* by reverse transcription quantitative PCR (RT-qPCR), where we detected ~250-fold higher levels of *FDX5* levels in wild type in comparison to *fdx5* (Supplemental Fig. S1; Supplemental Table S1). It should be noted that the *FDX5* knock-out strain contains a paromomycin cassette (with its own promoter and terminator) inserted within the second exon of *FDX5*. A major portion of the *FDX5* gene is still retained in the genome (Yang et al., 2015). A majority of the transcripts that we observed in the RNA-Seq data mapped to the region downstream of the insert and were ~10-fold lower in *fdx5* in comparison to wild type. This observation could be attributed to transcription from either the gene's

native promoter or from the paromomycin cassette promoter. Furthermore, the downstream location of the primers (Terauchi et al., 2009), with respect to the insert position within the gene (Yang et al., 2015), leads to detection of these run-off background transcripts in the RT-qPCR analysis.

We simultaneously analyzed the amounts of *FDX1*, *FDX2*, and *FDX5* proteins via immunoblotting, both before ($t = 0$) and after 48 h ($t = 48$) of S-deprivation. *FDX1* levels were higher in the *fdx5* strain in comparison to wild type at $t = 0$ (Tris-Acetate Phosphate plus sulfur [TAP+S]; Fig. 5D). At 48-h post -S conditions, the levels of *FDX1* decreased to approximately the same relative levels in both strains. Surprisingly, *FDX2* was detected exclusively in the *fdx5* later strain at $t = 0$, in contrast with its transcript down-regulation with respect to wild type at this same time point (Fig. 5, A and D). Absolutely no *FDX2* protein bands were observed in either strain at 48 h of incubation in S-depleted medium. Moreover, no *FDX5*-specific bands were detected in either strain at $t = 0$, although *FDX5* was specifically present in CC-124 at $t = 48$, which is consistent with up-regulation of *FDX5* under anaerobiosis (Terauchi et al., 2009). No corresponding bands were observed in the *fdx5* mutant strain at any time-point, which is consistent with it being a knock-out strain, despite showing partial transcript levels (see the previous paragraph). We also checked the levels of Rubisco and observed similar levels of RBCL protein expression in both strains under photoheterotrophic conditions ($t = 0$), and similarly reduced levels under S-starved conditions in both strains. To ensure similar protein loading, we ran in parallel a protein gel, which was stained with Coomassie Blue (Fig. 5D).

Global Transcriptome Profiling Reveals Differences in Gene Expression Related to the *fdx5* Phenotype

The global effect of S-deprivation on gene transcription in wild-type strains at various time points were previously reported by several groups (Nguyen et al., 2008; González-Ballester et al., 2010; Toepel et al., 2013). We performed a similar experiment but comparing the wild type to the *fdx5* strain and analyzing samples every 24 h from $t = 0$ through $t = 72$, when H_2 photo-production was first detected in the *fdx5* strain. Differences between wild-type and mutant were observed in transcripts in various pathways, details of which are shown in Supplemental Table S2. To relate transcriptional changes to the metabolic phenotype of *fdx5*, we focused on the specific pathways that were physiologically relevant to this study: photosynthesis, respiration, and carbon metabolism (both aerobic and anaerobic).

The lack of substantial effect of *FDX5* knock-out on photosynthetic electron transport rates under photoheterotrophic S-replete conditions was confirmed by the nearly equal level of gene transcripts involved in this pathway in both strains under S-replete, oxic

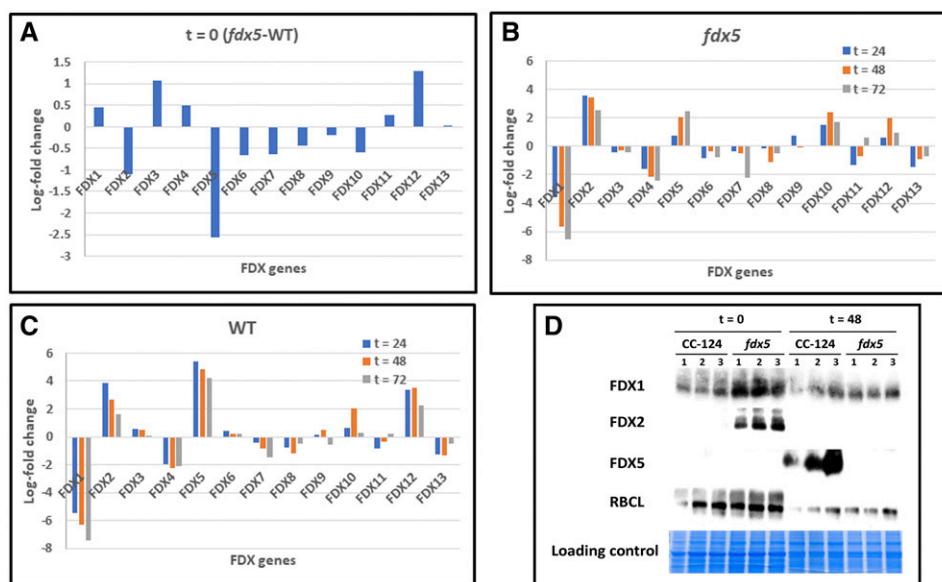


Figure 5. Expression of ferredoxins in response to sulfur starvation. A, RNA-Seq-based quantification of fold-changes of *FDX1–13* in *fdx5* at time points $t = 24, 48,$ and 72 in comparison to $t = 0$. B, RNA-Seq-based quantification of fold-changes of *FDX1–13* in wild type at time points $t = 24, 48,$ and 72 in comparison to $t = 0$. C, RNA-Seq-based quantification of fold-changes of *FDX1–13* at $t = 0$ between *fdx5* and wild type. Experiments were carried out in biological triplicates. WT, wild type CC-124. D, Immunoblotting of FDX1, FDX2, FDX5, and Rubisco large subunit (RBCL) proteins under S-replete ($t = 0$) and anoxic, S-deplete ($t = 48$) conditions. Equal amounts of protein were loaded in each lane as shown by Coomassie-stained gel run in parallel.

conditions (i.e. $t = 0$, Supplemental Fig. S2). As previously observed with the wild-type strain (Nguyen et al., 2008; González-Ballester et al., 2010), many photosynthetic genes were down-regulated after increasing periods of time under S-deprivation, while a few other transcripts increased in levels during the experiment (Supplemental Table S2; Supplemental Fig. S2) in both strains. Comparisons between wild type and *fdx5* also revealed a delayed response (either decrease or increase) in the levels of specific transcripts in *fdx5* during S-deprivation (Supplemental Fig. S2, red boxes). As expected, hydrogenases HYDA1 (Cre03.g199800.t1.1) and HYDA2 (Cre09.g396600.t1.1) transcript levels increased equally in both strains (Supplemental Fig. S2) in response to S-deprivation, which is required for H_2 production. Most interesting though, was the observation that the poly(A)-binding protein RB47 (Cre01.g039300.t1.2), which is required for initiation of the *psbA* mRNA translation, was found to decrease faster in wild-type than in *fdx5* (Supplemental Table S2)—which could contribute to the extended O_2 -production period in the mutant strain.

When analyzing the effect of the FDX5 knock-out mutation on the transcripts involved in the Calvin cycle (Supplemental Fig. S3), we observed a similar overall response to S-deprivation in both wild-type and mutant strains, consisting of a gradual decrease in a few transcript levels (albeit delayed in *fdx5*) as a function of time (red boxes), as reported by others for the wild-type strain (Nguyen et al., 2008; González-Ballester et al., 2010; Toepel et al., 2013), demonstrating the global consequences of the delayed response of

fdx5 to S-deprivation. No difference between the two strains were observed at $t = 0$.

In contrast, transcript levels of genes required for starch biosynthesis (Supplemental Fig. S4) increased equally in both strains except for Cre17.g721500.t1.2 (red boxes), encoding granule-bound starch synthase I, whose levels increased more quickly in *fdx5* than wild type during the 72-h process. No significant differences were observed at $t = 0$ between the two strains.

Transcripts of most enzymes catalyzing the reactions of glycolysis and TCA cycles were also only minorly affected in the *fdx5* strain (Supplemental Figs. S5 and S6). With respect to the carbon utilization enzymes, we specifically looked at the three isoforms of the acetate utilization pathway gene, ACS, which are found in *Chlamydomonas* (Supplemental Table S2; Supplemental Fig. S7), namely Cre07.g353450.t1.2 (ACS3), Cre01.g071662.t1.1 (ACS1), and Cre01.g055408.t1.1 (ACS2). While all three isoforms showed similar transcript levels at $t = 0$, only ACS1 was up-regulated over 2-fold in wild type and increased steadily up to 72 h. This gene was down-regulated ~ 1.5 -fold in *fdx5* during the first 24 h of S- starvation and to even lower levels at 48 and 72 h. Consistent with this observation, the ACS protein was detected in wild type even at 24 and 48 h, while being below detectable limits in the *fdx5* strain (Fig. 4). It should be noted that the commercially available ACS antibody used here does not differentiate between the different isoforms in *Chlamydomonas*.

Major differences in transcript levels between the two strains were seen in the fermentative pathway genes (Supplemental Fig. S8), particularly in transcript

Cre12.g543350.t1.1 encoding for formaldehyde dehydrogenase (FDH1), belonging to class III ADH family of proteins that catalyze the oxidation of formaldehyde to formate. This transcript is >5-logfold lower in *fdx5* at $t = 0$ and decreases further in this strain until 48 h of S-deprivation, while increasing ~5-logfold from $t = 0$ to $t = 72$ in the wild type. The lower levels of FDH1 transcripts in *fdx5* may reflect the slower establishment of anaerobiosis and explain the delayed detection of formate production by this strain. Additionally, the Cre01.g044800.t1.2 transcript (encoding the pyruvate formate lyase enzyme, PFL, which splits pyruvate into acetyl CoA and formate) spiked at 24 h but only in wild type, returning to lower levels afterward, which, again, may be related to the higher levels of formate produced by the wild type at earlier times. Finally, PFOR (Cre02.g095137.t2.1), which also catalyzes the breakdown of pyruvate into acetyl-CoA and CO₂, concomitant with fermentative H₂ production, was consistently found to be more up-regulated in wild type than in *fdx5* (Supplemental Table S2). The transcript profiles of these fermentative genes thus support the observation of delayed achievement of anaerobiosis in the mutant.

We also quantified the expression of the components of the thioredoxin (TRX) superfamily of proteins, which are involved in redox control of biochemical processes (Lemaire et al., 2004). We observed that only two out of 49 proteins annotated as TRX superfamily proteins were up-regulated in both wild-type and *fdx5* strain, one being the NADPH-dependent TRX reductase (NTR2, Cre02.g098850.t1.1, Supplemental Table S2). Besides NTR2, another NTR transcript, NTRC (Cre01.g054150.t1.2), showed slight up-regulation in both strains, but only after 48 h of S-starvation. It is worth noting that both NTR2 and NTRC proteins are NADPH-dependent, which agrees with the midpoint redox potential of FDX5 being closer to that of NADPH than FDX1 (Subramanian et al., 2018) and thus making it a good candidate for acting as an alternative electron partner or substitute under S-deprivation conditions.

Comparative Metabolome Analysis of Phenotype-Relevant Pathways

Because many genes are not regulated at the transcriptional level, we directly measured the content of various intracellular metabolites to determine the overall impact on the protein-mediated alterations to the wild-type and *fdx5* cultures harvested from $t = 0$ (S-replete, oxic), up to $t = 48$ after S-deprivation (S-deplete, anoxic; where maximum difference in physiology was observed between the two strains in this particular experiment). Supplemental Table S3 shows the changes in all quantified metabolites occurring in each strain during the process of S-deprivation.

With respect to one of the major products of photosynthesis, ATP, there is a clear overaccumulation of this nucleotide in the mutant strain relative to wild type, although its levels eventually decrease in *fdx5* at the end

of 48 h, possibly reflecting this strain's slower inactivation of photosynthesis and respiration. The levels of intracellular NAD⁺ in the wild type stayed above those in *fdx5* throughout the experiment, and more significantly so at 48 h (the assay was unable to differentiate between NAD⁺ and NADP⁺), correlating with the lower photosynthetic activity of the wild-type strain at this time point.

The quantification of glycolytic intermediates (Supplemental Table S3) showed mixed results, with Fru-1,6-bisphosphate (FBP) peaking in the mutant strain at $t = 24$ and both 2,3-phosphoglycerate and phosphoenolpyruvate peaking at $t = 48$. Ribose-1,5-bisphosphate is known to be a regulator of FBP and Fru-6-phosphate in the liver (Sawada et al., 2000). Consistent with higher FBP levels, Ribose-1,5-bisphosphate amounts were also statistically higher in *fdx5*. The levels of pyruvate, on the other hand, start higher in *fdx5* but gradually decrease to wild-type levels during the 48-h period.

TCA cycle intermediates were present in higher levels in *fdx5* and decreased below wild-type levels in most cases by 48 h of S-deprivation. Lactate, the intracellular fermentative metabolite and alternative electron sink in glycolysis, was also quantified and showed almost 2-fold lower levels in *fdx5* in comparison to wild type, with maximum production in wild type observed at $t = 48$. However, this metabolite was not detected in the extracellular environment in either of the strains, based on our HPLC analysis.

With respect to the amino acids, Ser, Met, Arg, Glu, and Gln levels peaked at $t = 6$ and then decreased in both strains (suggesting a direct response to S-deprivation), while Phe, Trp, Thr, Asp, and Ala increased only after 24 h of S-deprivation (possibly related to the start of anaerobiosis).

Identification of FDX5 Interactors Using Pull-Down Assays

To probe for possible FDX5 interactors that would be consistent with the observed physiological changes, we performed pull-down assays using heterologously expressed FDX5 from *Escherichia coli* (Peden et al., 2013) covalently coupled to CNBr sepharose as bait and protein extracts from wild-type cultures exposed to photoheterotrophic (aerobic, S-replete), 30-min anaerobic incubation, and 6-h post-anoxia under S-deprivation conditions. Supplemental Table S4 shows the complete list of proteins identified by mass spectrometry (MS), while Table 2 shows the major interactors of FDX5 under the three different test conditions.

Most interactors identified in this assay were present exclusively under either S-deprivation or anaerobic conditions (Table 2), where the FDX5 gene is expressed at higher levels, and a few of them were present in large amounts under both conditions, such as HYDEF and FDX5 (detected FDX5 protein is most likely protein leaching off the Sepharose [GE Healthcare] beads). The

Table 2. Major FDX5 protein interactors identified by pull-down analysis using cell extracts of CC-124 cells grown under aerobic, anaerobic, and sulfur-deprived (6 h into anoxic phase) conditions

The peptide ratio given is corrected for total number of peptides found in the sample versus that of the negative control. Ribosomal proteins are not listed. Bold numbers represent interactors considered important under the tested culture conditions (S-deprivation). Numbers in parentheses represent peptides found in the sample and negative control, respectively. Only proteins with an at least 2-fold increase over no-protein control are listed.

Gene Accession Number	Protein Descriptor and Gene Name	Peptide Ratios FDX5/Ctrl ^a (Absolute Peptide Counts Shown in Parentheses)		
		Aerobic	Anaerobic	–Sulfur
Photosynthesis-Related				
Cre10.g420350.t1.2	PSI 8.2 kD reaction center subunit IV (PSAE)	1.37 (2/2)	0.78 (2/4)	2.54 (2/1)
Cre08.g362900.t1.3	PSII PSBP-like protein (PSBP4)	0 (0/1)	0.78 (1/2)	2.54 (2/1)
Cre03.g199800.t1.1	HYDA1 hydrogenase	1.1 (4/5)	1.16 (3/4)	1.9 (6/4)
Cre06.g296750.t1.2	Iron hydrogenase maturation protein (HYDEF)	0.69 (1/2)	3.1 (2/1)	2.54 (2/1)
Cre02.g098850.t1.1	NADPH-dependent thioredoxin reductase (NTR2)	0.69 (1/2)	0 (0/0)	3.38 (8/3)
Glycolysis/TCA Cycle/Respiration				
Cre12.g485150.t1.2	Glyceraldehyde 3-P dehydrogenase (GAP1)	4.12 (9/3)	15.51 (10/1)	3.08 (17/7)
Cre06.g282800.t1.2	Isocitrate lyase (ICL1)	0.17 (1/8)	0 (0/3)	2.54 (2/1)
Cre12.g514750.t1.2	Citrate synthase (CS11)	0 (2/0)	0 (1/0)	3.81 (3/1)
Cre07.g327400.t1.1	NADH:ubiquinone oxidoreductase subunit (NUO9)	0 (0/1)	3.1 (2/1)	1.9 (3/2)
g14920.t1	Succinate dehydrogenase	0.69 (1/2)	0 (0/1)	2.12 (5/3)
Cre16.g691850.t1.2	Cytochrome c oxidase subunit (COX90)	1.83 (4/3)	1.55 (3/3)	2.54 (4/2)
Cre07.g338050.t1.2	Mitochondrial F1F0 ATP synthase associated 36.3 kD protein (ASA3)	1.14 (5/6)	0.62 (2/5)	5.08 (4/1)
Cre12.g535950.t1.2	NADH-ubiquinone oxidoreductase 76 kD subunit (NUOS1)	0 (1/0)	1.55 (1/1)	2.12 (5/3)
Oxidative Pentose Phosphate Cycle				
Cre08.g378150.t1.3	Glc-6-P dehydrogenase (GLD2)	0 (0/0)	0 (1/0)	2.54 (4/2)
Lipid Metabolism				
Cre17.g701700.t1.2	PFO2770 Plastid acyl-ACP desaturase	4.51 (23/7)	2.77 (25/14)	3.81 (12/4)
Cre03.g158900.t1.2	Dihydrolipoamide acetyltransferase (DLA2)	1.65 (6/5)	1.16 (6/8)	2.54 (4/2)
Protein Glycosylation				
Cre03.g169400.t1.2	UDP-D-glucuronic acid decarboxylase (GAD1)	0.92 (2/3)	1.55 (2/2)	2.54 (2/1)
Polysaccharide Biosynthesis				
g9579.t1	PFO4321-PFO1370-PFO2719 NAD-dependent epimerase/dehydratase family	0.34 (1/4)	0 (0/7)	2.54 (2/1)
ROS Remediation				
Cre06.g271200.t1.2	Monodehydroascorbate reductase	0 (0/0)	0 (0/0)	2.54 (2/1)
Cre07.g319100.t1.3	Glutathione S-transferase-related protein (TEF18)	0 (1/0)	0 (0/0)	2.54 (2/1)
Cre01.g014350.t1.2	Peroxiredoxin type II (PRX5)	0 (0/0)	0 (0/1)	2.54 (2/1)
Cre12.g553700.t1.2	Glutathione S-transferase kappa (PDO2)	2.75 (2/1)	0 (3/0)	1.27 (2/2)
Nitrogen/Amino Acid Metabolism				
Cre07.g334800.t1.2	Ferredoxin (FDX4)	9.61 (7/1)	6.98 (9/2)	12.69 (10/1)
g9648.t1	Asp semialdehyde dehydrogenase (ASD1)	1.72 (5/4)	1.86 (6/5)	6.35 (5/1)
Cre09.g416050.t1.2	Argininosuccinate synthase (AGS1)	0 (0/3)	0 (0/5)	3.81 (3/1)
Others				
Cre17.g700950.t1.2	Apoferredoxin 5 (FDX5)	23.35 (51/3)	91.52 (59/1)	68.53 (54/1)
g8568.t1	Sulfite reductase (SIR4)	0 (0/0)	0 (0/0)	2.54 (2/1)
Cre09.g407700.t1.2	Cys endopeptidase (CEP1)	1.37 (1/1)	0 (3/0)	5.08 (16/4)
Cre01.g000350.t1.3	p-hydroxybenzoate hydroxylase (OXR1)	0 (1/0)	1.55 (1/1)	2.54 (2/1)
Cre02.g073200.t1.2	Thr deaminase (THD1)	1.83 (4/3)	2.07 (4/3)	8.88 (7/1)
g9773.t1	Guanylate kinase	2.75 (2/1)	0.39 (1/4)	3.81 (3/1)
Cre12.g508900.t1.2	MAPK (MAPK6)	4.81 (7/2)	3.1 (6/3)	6.98 (11/2)
Cre17.g709550.t1.2	Jumonji domain-containing protein	1.37 (1/1)	0.78 (1/2)	2.54 (2/1)
g13844.t1	Selenophosphate synthetase	0 (0/1)	0 (0/1)	4.44 (7/2)
Cre06.g284900.t1.2	Peptidyl-prolyl cis-trans isomerase	2.75 (2/1)	0 (1/0)	3.81 (3/1)
Cre03.g172000.t1.2	3-oxoacyl-[acyl-carrier protein] reductase	2.06 (3/2)	4.65 (6/2)	3.81 (3/1)
Cre15.g635600.t1.2	Nascent polypeptide-associated complex subunit alpha (NPC1)	2.06 (3/2)	3.1 (2/1)	3.81 (3/1)
Cre02.g079700.t1.2	Asp carbamoyltransferase (PYR2)	1.83 (4/3)	1.24 (4/5)	3.81 (3/1)
Cre17.g716400.t1.2	Pre-60S factor REI1 (REI1)	0 (0/1)	1.55 (2/2)	3.81 (3/1)
Cre12.g544150.t1.2	Peptidyl-prolyl cis-trans isomerase	0 (0/1)	0 (0/1)	3.81 (3/1)
Cre13.g607050.t1.2	Thiosulfate sulfurtransferase (THT1)	0 (0/0)	0 (0/0)	3.81 (3/1)
Cre12.g522450.t1.2	COP-II coat subunit (SEC31)	2.75 (4/2)	0 (3/0)	3.17 (5/2)
Cre09.g406600.t1.1	Unknown function	0 (0/0)	0 (0/0)	3.81 (3/1)

^aRatio was presented as "0" when the peptide count in either the sample or the control was below detection limits (i.e. 0).

assay revealed an interaction with HYDA1, particularly under S-deprivation, but other known ferredoxin interaction partners such as PFOR and HYDA2 could not be detected at sufficient levels. As expected, most of the interactors are redox enzymes, although not all of them are located in the chloroplast (e.g. NUOS1 and COX90). This emphasizes the fact that nonspecific and “false-positives” interactors may be identified and that the results were therefore considered only in the context of other experimental evidences. The interactor NTR2 is a chloroplast-localized protein, involved in the reduction of TRXs that can in turn activate the first step in starch synthesis, thus making this particular interaction of major interest to our work given the physiological response of the mutant to S-deprivation during its aerobic phase. Moreover, some of the identified interactors have also been shown to have a delayed response to S deprivation at the transcriptional level in the mutant strain, namely ACS3 (Table 2; Supplemental Table S4).

Finally, the pull-down assay identified four additional chloroplast-localized redox enzymes as major FDX5 interactors under S-deprivation (Table 2). The first three, monodehydroascorbate reductase, TEF18, and peroxiredoxin5, are components of the glutathione cycle; the glutathione cycle is known to affect cell division, cell death, and light signaling, among its other functions (Buchanan, 2016). These functions also correlate with the lack-of-growth in the dark phenotype of the mutant (Yang et al., 2015). The fourth interactor identified was FDX4, a chloroplast-localized ferredoxin of unknown function.

DISCUSSION

Delayed Response of Photosynthetic and Fermentative Metabolism to Sulfur Deprivation in *fdx5*

One of the most striking observations made in this work was the delay in establishment of anaerobic metabolism upon S-deprivation by *fdx5* when compared to the wild type, as demonstrated by changes in photosynthesis and respiration rates, levels of O₂ in the headspace, production of H₂, and accumulation of fermentative metabolites. Because the O₂ consumption, respiration capacities, and net O₂ evolution are similar between *fdx5* and wild type at $t = 0$ (S-replete conditions) under the experimental light intensity (100 $\mu\text{E m}^{-2} \text{s}^{-1}$; Table 1), this suggests that the observed slower decrease in O₂ levels, post S-deprivation in *fdx5* (Fig. 1B), must be caused by extended O₂ evolution in this strain, resulting from slower de-activation of PSII as shown by higher net O₂ evolution rate in this strain. In this context, we observed that the transcript levels of the poly(A)-binding protein RB47, which is part of a complex that binds to the 5' untranslated region of the *psbA* mRNA (encoding the PSII protein D1) and is required for *psbA* translation initiation, decrease much more slowly in *fdx5* upon S-deprivation. The RB47 protein

was shown to directly affect the accumulation of the PSII reaction center polypeptide D1 (Yohn et al., 1998; Alizadeh and Cohen, 2010). Furthermore, immunoblots showed that the D1 protein levels decreased much more slowly in *fdx5* than in the wild-type strain (Fig. 4) suggesting extended activity of the PSII reaction center in the mutant strain. It has also been further suggested that binding of RB47 to *psbA* mRNA is modulated via RB60, which in turn is redox-controlled by FDX–TRX interactions. This redox-mediated control of D1 protein synthesis, in combination with its sustained expression and detection in *fdx5*, supports the observed slower achievement of anaerobiosis in *fdx5* in comparison to wild type under S-deprivation (Fig. 1B), and indicates that the process requires FDX5 activity.

An additional result of the delayed S-deprivation response is also provided by the higher levels of ATP at $t = 24$ in the mutant strain (Supplemental Table S3), reflecting the mutant's slower inactivation of photosynthetic O₂ evolution and respiratory O₂ consumption compared to CC-124.

Despite its presence in the medium, acetate is consumed only during the aerobic phase and not during anaerobiosis by this alga (Melis et al., 2000; Tsygankov et al., 2002; Kosourov et al., 2003). The acetate consumption rate in *fdx5* was significantly slower in comparison to wild type during their respective oxic phases, remaining active in *fdx5* up until 72 h (Fig. 3), possibly because of extension of the aerobic phase.

Besides anaerobiosis, it is known that intracellular accumulation of starch during the initial phase of S-deprivation is crucial for sustained H₂ production in *Chlamydomonas* (Melis et al., 2000; Kosourov et al., 2003). Thus, the delayed response of the mutant to S-deprivation could be explained by three additional concurrent factors:

- (1) The transcript levels of one of the three ACS genes (*ACS1*, Cre01.g071662.t1.1) was down-regulated in *fdx5* at all time points past $t = 0$, while being up-regulated in wild type starting at $t = 24$ (Supplemental Table S2).
- (2) The ACS protein levels were lower in *fdx5* in comparison to wild type in the oxic phase ($t = 6$), while being detectable only in wild-type strain at 24- and 48-h post S-deprivation (Fig. 4). The *fdx5* strain showed barely detectable levels at $t = 24$ and $t = 48$.
- (3) Initial starch accumulation, which is the major substrate for respiration and fermentation during the anoxic phase of S-deprivation (Fig. 3), was at least 2-fold higher in wild type in comparison to *fdx5*. This was consistent with higher protein levels of the starch synthesis enzyme, AGPase, at $t = 24$ in wild type (Fig. 4). On the other hand, *fdx5* showed prolonged but lower levels of starch accumulation, as supported by its detection even at $t = 48$, while not being detected in wild type at the same time point.

In this context, it is worth mentioning that ACS1 is predicted to be localized to the cytoplasm, based on the prediction software “DeepLoc-1.0” (www.cbs.dtu.dk/services/DeepLoc/), and is classified under the “other” category based on the prediction software “PredAlgo” (<https://giavap-genomes.ibpc.fr/cgi-bin/predalgotdb.perl?page=main>). This enzyme catalyzes the first step in acetate utilization (i.e. conversion of acetate to acetyl-CoA). ACS is a redox-regulated protein with known interaction with TRX (Lemaire et al., 2004), thereby suggesting that its lower functionality in the *fdx5* mutant could also be due to a lack of electron donation from FDX5 to the TRX.

The observation regarding differences in starch accumulation between wild-type and *fdx5* is further consistent with two additional findings. First, based on previous pull-down assays, FDX5 was shown to interact with the starch-branching enzyme SBE3 (Peden et al., 2013), PF02373 glycosyl transferase, UDP-D-glucuronic acid decarboxylase (GAD1), and Nicotinamide adenine dinucleotide (NAD)-dependent epimerase/dehydratase enzymes (Table 2), all of which are involved in starch biosynthesis. These interactions suggest FDX5’s direct role in this process, through still unknown redox-mediated mechanisms. Nevertheless, we observed that SBE3 (Cre10.g444700.t1.1) showed >2-fold higher transcript levels during the first 24 h of S-starvation in both wild-type and *fdx5*, while starting at very low levels in *fdx5* at $t = 0$ (Supplemental Table S2), exemplifying posttranscriptional regulation in the mutant. Interestingly, however, it is also known that the Arabidopsis (*Arabidopsis thaliana*) starch branching enzyme AtBE2, which is a homolog of SBE3, is only active under reducing conditions and is a known TRX target (Glaring et al., 2012). A second evidence for the role of FDX5 in starch biosynthesis was the observation that overexpression of FDX5 increases starch accumulation in *Chlamydomonas* (Huang et al., 2015). Finally, a third piece of evidence is based on RNA-Seq analysis, whereby NTR2 was found to be up-regulated under $-S$ conditions in both *fdx5* and wild type. Based on the pull-down experiments, FDX5 interacts with NTR2, an enzyme that activates the first reductive step in the starch biosynthesis pathway involving the AGPase enzyme STA6 (Michalska et al., 2009). This strongly suggests that lower starch accumulation in *fdx5* may also be a consequence of the role of FDX5 in providing reductant to NTR2. To test this hypothesis, we obtained the NTR2-disrupted mutant from the *Chlamydomonas* mutant collection library and tested starch levels in this mutant within the first 24 h of S-deprivation, i.e. time point at which maximum effect of starch synthesis is observed in wild type. No reduction in starch levels was observed in this strain, suggesting that interaction of NTR2 with FDX5 is not essential for AGPase function under these conditions (V. Subramanian and M.S.A. Wecker, unpublished data). However, further investigation on the NTR2 mutant and its genotype would be needed to confirm this observation. The STA6 transcript (Cre03.g188250.t1.2) itself, though, did not

show significant quantitative changes in the two strains under the tested conditions (Supplemental Fig. S4)—evidence that this protein’s function is not regulated at the transcriptional level. Thus, it is likely that FDX5-mediated regulation of STA6 occurs via its interactions with TRXs.

Our data suggest that the delay in establishment of anaerobiosis and starch metabolism in *fdx5* is also responsible for delayed photoproduction of H₂, formate, CO₂, and ethanol (Figs. 1 and 3). The difference in the amount of starch accumulated during the aerobic phase has been shown to affect the final H₂ photoproduction levels (Posewitz et al., 2004) and it could explain the low amount of H₂ produced by *fdx5*, which yielded ~40% of total H₂ compared to the wild-type strain at the end of 120 h of S-deprivation. Similarly, slower accumulation of other fermentative metabolites could also be a result of slower starch accumulation in *fdx5*. However, it should also be noted that one of FDX5’s interaction partners is the hydrogenase HYDA1 and its maturation, the S-adenosylmethionine-radical protein HYDEF (Peden et al., 2013). This suggests the formation of a complex among HYDA1, HYDEF, and FDX5 during hydrogenase maturation, which could not occur in the *fdx5* mutant. As of now, the occurrence of this interaction has not been demonstrated and would need further investigation. Slower and lower accumulation of the other fermentative metabolites, on the other hand, was also consistent with the lower induction of *PFL*, *PFOR*, and *FDH* in *fdx5*, as well as the lower levels of *PFOR* and *ADH1* proteins in *fdx5*, highlighting the transcriptional-level control of these pathways.

Additional Proposed Roles for FDX5 Based on Omics and Protein Interaction Studies

The midpoint potential of FDX5 (−320 mV) is favorable for its interaction with both NAD(P)⁺ and TRXs and thus is capable of reductively activating these species and through them posttranscriptionally regulating various metabolic enzymes. TRXs-dependent redox regulation is well-known in photosynthetic systems. In *Chlamydomonas*, it has been shown that TRX-mediated regulation is involved in various processes such as activation of the TCA cycle and the Calvin cycle, amino acid biosynthesis and fatty acid biosynthesis, the nitrogen- and S-assimilation pathways, and in reactive oxygen species detoxification and protein folding (Lemaire et al., 2004). Here, we propose that the redox state of chloroplast-localized FDX5 may affect the transcription of various nuclear genes, given the observed interaction between FDX5 with the transcriptional regulator MAPK6 (Table 2), through still unknown mechanisms.

In this study, a few proteins were shown to be regulated both at the transcriptional and posttranslational levels in our experiments as, for example, ACS1, as discussed in the “Delayed Response of Photosynthetic and Fermentative Metabolism to Sulfur Deprivation in

fdx5" section. Similarly, transcriptional regulation was accompanied by consistent changes in their function in the case of the fermentative enzymes FDH1, PFL, and PFOR, whose reaction products increased more slowly in the *fdx5* strain, thus reiterating the possible role for FDX5 in their transcriptional regulation.

On the other hand, our results showed that glyceraldehyde-3-phosphate dehydrogenase (GAP1) and glucose-6-phosphate dehydrogenase (GLD2) are regulated post-translationally by FDX5. This is based on the observation that, while GAP1 (Cre12.g485150.t1.2) transcript levels were low in *fdx5* and GLD2 levels were high in both wild-type and *fdx5* strains, both showed interaction with FDX5 in the pull-down assays. However, the product of these two pathway reactions were found to be higher in *fdx5*, suggesting a more prominent role of posttranslational regulation under these conditions. Although further experimental evidence is needed to show the ability of FDX5 to reduce these proteins, it is highly likely that FDX5 could be playing an alternate role to NADPH, TRXs, or glutathione, particularly under anoxic, S-deprivation conditions. This discrepancy between transcript regulation and control of enzyme activity was also observed in the case of FDX2, where the protein was detected at $t = 0$ only in *fdx5*, while its transcript levels were lower in *fdx5* at that time point. However, as transcript levels increased in both strains during S-deprivation (Fig. 5, B–D; Supplemental Table S2), no protein was detected in the immunoblot analysis in either strain. Similar disagreement between transcriptional and translational levels were also reported by Terauchi et al. (2009). Detection of FDX2 in the mutant strain at $t = 0$ (S-replete conditions) suggests a possible compensatory or a unique role of this ferredoxin under FDX5-null conditions. However, the specific role of this protein in this mutant strain would need further investigation.

Another example of complex regulatory control by FDX5 is exemplified by the case of the fatty acid (FA) desaturases CrFAD6 and CrΔ4FAD, which were shown to interact with FDX5 (Yang et al., 2015), while being down-regulated during S-deprivation in *fdx5* (Supplemental Table S2). The *fdx5* strain was shown to have aberrant thylakoid membrane structure when incubated in the dark, which was attributed to the decreased unsaturated FA levels (Yang et al., 2015). However, this study showed no changes in structural integrity of cells in the mutant strain when exposed to S-depleted conditions (Fig. 2); in fact, mutant cells appeared bigger under both photoheterotrophic and S-deprivation conditions for still unknown reasons. A similar observation was made in *Synechocystis* PCC6803, where deletion of one of the ferredoxins, *fed2*, resulted in increased cell size (Cassier-Chauvat and Chauvat, 2014). Clearly, dark stress versus a combination of anaerobic and nutrient stress (such as –S) induce a different response in the mutant strain that is not dependent on FDX5's interaction with the FA desaturases.

It appears that deletion of FDX5 slows down the response of the cells to S stress, leading to slow depletion of the S reserves followed by its increased cell viability when compared to the wild-type strain. A combination of prolonged O₂ evolution activity and decreased carbon metabolism in *fdx5* results in slower acclimation to S-deprivation. Overall, results suggest that several biochemical pathways are regulated by interaction of FDX5, either directly or indirectly via TRXs, which is otherwise absent in the *fdx5* mutant, resulting in the slow "S-phenotype" of this strain. Interestingly, deletion of FDX5 does not result in a nongrowth phenotype under S-deprived conditions, as observed under dark conditions, suggesting its more subtle role as a redox-partner under the former

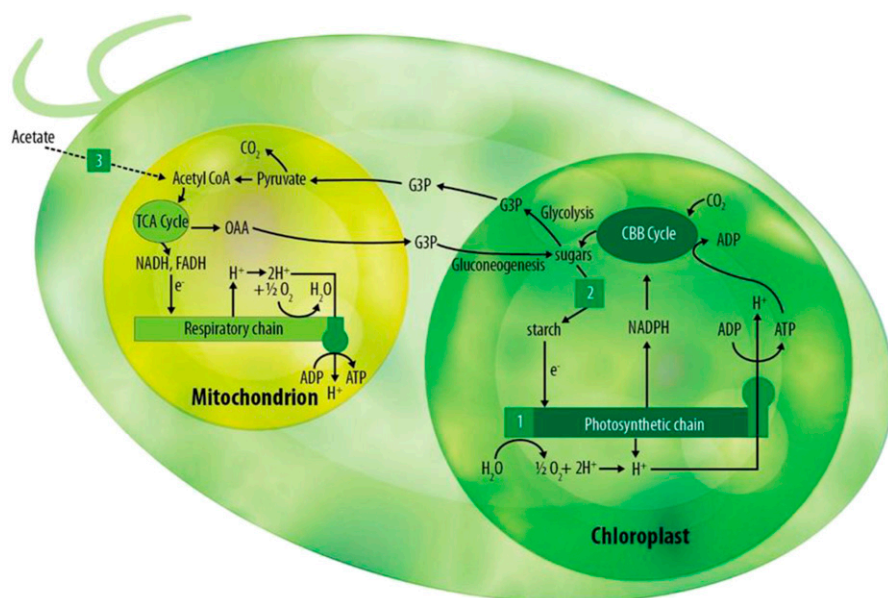


Figure 6. Schematic representation of the role of FDX5 in specific pathways in *Chlamydomonas* under S-deprived conditions. Metabolic pathways functioning in the different organelles (chloroplast and mitochondria) in *Chlamydomonas* are presented (Johnson and Alric, 2013). Numbers represent the three specific pathways where physiological effects of FDX5 deletion has been demonstrated experimentally: 1, PsbA-involving photosynthetic electron transfer pathway; 2, starch synthesis pathway; 3, acetate utilization pathway. CBB, Calvin-Benson-Bassham; G3P, glyceraldehyde 3-phosphate; OAA, oxaloacetate.

conditions, which could be likely replaced by other ferredoxins.

CONCLUSION

We have shown that FDX5 is involved directly or indirectly in several functions in *Chlamydomonas*. One of the major results from this work is the delayed response of *fdx5* to S-deprivation probably because of its role in *psbA* translation initiation, and regulation of acetate and starch metabolism pathways. Our evaluation of the physiological characteristics of the *fdx5* mutant under S-deprivation, in combination with transcriptomics, metabolomics, and pull-down assay experiments confirmed its observed phenotype and also suggests additional roles for FDX5 in transcriptional and/or posttranslational activation of genes in *Chlamydomonas*, which deserves further investigation.

Our results explain the *fdx5* mutant phenotype under S-deprivation as follows: In response to S-deprivation, FDX5 transcription in the wild type is induced even under the aerobic phase (Zalutskaya et al., 2018), which allows *psbA* mRNA translation (coding for D1 protein) occurring simultaneously with the lack of D1 repair, resulting in the well-known gradual decrease in photosynthetic activity. Because of the lack of FDX5 in the knock-out mutant, *psbA* translation is probably maintained for longer periods of time, thereby delaying anaerobiosis. Moreover, the establishment of anaerobiosis under S-deprivation is dependent on the balance between photosynthetic O₂ evolution and respiratory O₂ consumption. Because both *psbA* translation and acetate uptake are affected in *fdx5*, the onset of anaerobiosis is delayed in this strain.

Besides its effect on photosynthesis and respiration, S-deprivation induces accumulation of starch in wild-type algae during the initial aerobic phase. In *fdx5*, starch synthesis is slower and total accumulated levels are much lower. We have demonstrated that this phenotype might also be a direct consequence of decreased carbon uptake in the form of acetate by *fdx5*, which is a result of lower ACS protein levels. Moreover, lower starch accumulation could also be partially attributed to lower TRX-mediated posttranslational reduction of STA6, resulting in extended periods and lower levels of STA6 protein synthesis. Additionally, the lack of FDX5 in the mutant could influence the levels of activities of other starch synthesis-related enzymes, such as SBE3. Because starch is an electron and carbon source under anaerobiosis, reduced starch accumulation during the aerobic phase, in turn, affects downstream pathways such as fermentative metabolism and H₂ photoproduction. Lower H₂ production (photo and fermentative) could also result from the lack of FDX5's tripartite interaction with HYDA1 and HYDEF and/or lower expression of PFOR in the mutant strain, which is required for ferredoxin reduction during fermentative H₂ production. Thus, fermentative pathways are directly or indirectly affected, and their

activities delayed in *fdx5*. Lower accumulation of fermentative metabolites was also supported by the observed delay in transcription and lower protein levels of the fermentative pathway enzyme ADH1 in the *fdx5* mutant. The role of FDX5 in specific pathways when grown under S-deprived conditions, is summarized in Figure 6.

In addition, we have shown that FDX5 may also play an important role in activity of proteins such as GLD2 and GAP1, both of which are known to be regulated by TRXs, and we have demonstrated that alternative ferredoxins such as FDX2, whose levels increased in *fdx5* under photoheterotrophic conditions, may play compensatory roles in the absence of FDX5 in *Chlamydomonas* under these conditions. Further work involving a double *fdx5/fdx2* mutant could address this issue in the future.

MATERIALS AND METHODS

Cultures and Strains

CC-124 (*nit1*⁻, *nit2*⁻, *mt*⁻) was routinely maintained on TAP medium at 25°C with constant illumination at 40 μE m⁻² s⁻¹ photosynthetically active radiation (PAR). The *fdx5* strain was obtained from Dr. Arthur Grossman's laboratory at the Carnegie Institute, which had been backcrossed five times to CC-124 and CC-125 (*nit1*⁻, *nit2*⁻, *mt*⁺; Yang et al., 2015). The mutant strain was maintained on TAP solid medium containing hygromycin (10 μg/mL).

Photosynthesis and Respiration Measurements

Chlamydomonas reinhardtii (hereafter *Chlamydomonas*) cultures were grown in Roux bottles with constant CO₂ bubbling to a chlorophyll content of ~20 μg/mL. A 2-mL aliquot was directly transferred to the Clark Electrode Chamber (ALGI) to which 50 μL of 0.5-M NAHCO₃ was added and allowed to incubate for 30 s in the dark before illuminating with different light intensities (50–2,000 μE m⁻² s⁻¹ PAR) for 1 min for measurement of O₂ evolution rates. Respiratory O₂ consumption rates were measured by subjecting the cultures to the dark for 1 min at the end of the illumination period. Net photosynthetic rates were calculated by subtracting the rates of dark respiration from the measured O₂ evolution rates. To measure respiration under anaerobic conditions, O₂ gas was added to the sample to ~6% (by first adding a slight excess of O₂ and then adding argon until a reading of 0.7 V). All experiments were carried out in biological triplicates.

Anaerobic Induction via Sulfur Deprivation

Algal cultures were grown in 1-L Roux flasks containing 750 mL of TAP liquid medium at 100 μE m⁻² s⁻¹ PAR with constant stirring at 25°C until they reached a chlorophyll content of ~20 μg/mL. Cultures were centrifuged at 3,500g for 5 min and washed with TAP lacking sulfur (TAP-S) medium. This procedure was repeated thrice before a final resuspension of the cells in 140 mL of TAP-S medium at a concentration of 20 μg/mL. At this point, the cultures were transferred to 150-mL screw-capped bottles containing rubber septa for anaerobic induction and incubated with stirring under 100 μE m⁻² s⁻¹ PAR illumination for 96–120 h. The H₂ gas generated during the anaerobic phase was not released, although 400 μL was used for quantification per the procedure mentioned under the "CO₂, O₂, and H₂ Measurements" section. Three independent biological replicates were used for the S-deprivation experiments.

CO₂, O₂, and H₂ Measurements

One milliliter of cells from -S cultures were transferred with a gas-tight syringe to a 7-mL sealed vial containing 1 mL of 1-M HCl. This suspension was shaken to liberate CO₂ to the headspace. Quantification of CO₂ was performed by gas chromatography (GC, model no. 5890 Series II Gas

Chromatograph; Hewlett Packard) using a Supelco column (80/100 PORAPAK N1.82 m × 3.175 mm × 2.1 mm; Sigma-Aldrich) coupled to a thermal conductivity detector. Total H₂ and O₂ levels were measured by analyzing 400 μL of head-space gas by GC (model no. 7890 System; Agilent Technologies) using a Supelco column (60/80 mol sieve 5A 1.82 m Ft × 3.175 mm; Sigma-Aldrich) coupled to a thermal conductivity detector. Data were obtained from three independent –S cultures.

Extracellular Metabolite Analysis

Extracellular metabolite analysis was done as published in Dubini et al. (2009). One milliliter of cells were harvested using a sterile syringe from cultures exposed to –S from $t = 0$ through $t = 96$. Cells were pelleted and the supernatant was transferred to a microcentrifuge tube. Both the pellet and the supernatant were snap-frozen in liquid nitrogen and were subsequently used for both starch (see "Starch Analysis" section) and metabolite analysis. HPLC analysis was performed using a model no. 1200 Series System (Agilent Technologies). Briefly, 100 μL of filtered sample was injected into a model no. HPX-87H (300 × 7.8 mm) ion-exchange column (Aminex). Metabolites were separated at 65°C with 4 mM of sulfuric acid as the mobile phase at a flow rate of 0.4 mL/min. Retention peaks for the various organic acids were recorded using the software "ChemStation" (Agilent Technologies), and quantifications were performed by comparisons with standard curves of known organic acid standards.

Starch Analysis

Frozen cell pellets from three biological replicates were thawed, and chlorophyll extracted by vortexing with 95% (v/v) ethanol. The pellets were then washed twice with 0.1 M of sodium acetate at pH 4.5, resuspended in 0.5 mL of the same solution, and transferred to screw-capped cryo vials (Thermo Fisher Scientific), and autoclaved for 20 min. Amyloglucosidase solution (Sigma-Aldrich) was added to the vials at a final concentration of 8 units/mL, and the mixture was incubated at 55°C overnight. We assayed 10 μL from each vial for Glc concentration, using the GAHK-20 Sigma Kit (Sigma-Aldrich). Starch concentration was measured as micromoles of Glc equivalent (180.2 g/mol).

Immunoblotting

Cells pellets obtained from 0- and 48-h post –S deprivation were resuspended in 1 mL of protein extraction buffer (10 mM of Tris-Cl at pH 7.5, 1 mM of EDTA, and 0.5 mM of dithiothreitol) containing 0.1-mM phenylmethanesulfonyl fluoride and a 1:1,000 diluted protease inhibitor cocktail (Sigma-Aldrich). This cell suspension was subjected to sonication using 10 intervals of 30-s duration each, with 30-s intermittent cooling on ice. The extracted protein solutions were clarified by sequential centrifugation from 6,000g to 15,000g for 10 min, followed by storage at –80°C for future use. Total protein content was measured using the Bradford reagent protocol (Bio-Rad). Alternatively, cells were resuspended in protein extraction buffer containing 50 mM of Tris at pH 8.0, 2% (w/v) SDS, 10 mM EDTA, and protease inhibitors followed by vortexing and centrifugation at 6,000g for 5 min (Fig. 4). Protein concentration was determined by bicinchoninic acid assay (Thermo Fisher Scientific). Equal protein amounts were separated by SDS-PAGE and then transferred to nitrocellulose membranes. A parallel gel was subjected to Coomassie blue staining to determine the protein loading in the blots. Membranes were then probed with rabbit polyclonal antibodies and the target proteins detected using horseradish-peroxidase conjugated secondary antibody (Thermo Fisher Scientific). Antibodies against FDX1, FDX2, STA6/AGPase, and Rubisco large subunit were obtained from Agrisera. The ADH1 and PFOR antibodies were obtained from Arthur Grossman's laboratory (Carnegie Institute). The ACS antibody raised against human ACS enzyme (cat. no. 16087-1-AP) was obtained from Proteintech. FDX5 antibody was custom-raised against the whole protein in rabbit.

Transcriptomics Analysis by RNA-Seq

Total RNA for RNA-Seq analysis was obtained as follows. Cultures were grown to ~20-μg Chl/mL (unless otherwise indicated). A 7.5-mL volume of culture was pelleted by centrifugation and immediately resuspended in 560 μL of PureLink Plant RNA Reagent (Thermo Fisher Scientific), and transferred to a 1.5-mL Eppendorf tube. The reaction was rocked gently for 5 min and then centrifuged for 2 min at 13,000 rpm. A 500-μL aliquot of the supernatant was

then transferred to a new 1.5-mL tube to which 100 μL of 5-M NaCl and 400 μL of chloroform were added. The mixture was again briefly vortexed and centrifuged for 5 min at 13,000 rpm. A 400-μL aliquot of the supernatant was then transferred to a new 1.5-mL tube to which 400 μL of isopropanol was added and incubated for 10 min at room temperature. The mixture was again centrifuged at 13,000 rpm for 10 min at room temperature to pellet the RNA. This pellet was washed with ice-cold 70% (v/v) ethanol before final resuspension in 100-μL RNase free water. This RNA solution was cleaned further by passing it through an RNeasy column (Qiagen) followed by DNase treatment. This reaction mixture was purified over a second RNeasy column (Qiagen) and the final product was analyzed on an agarose gel.

RNA samples were submitted to the Genomics and Microarray Core Shared Resource of the University of Colorado Cancer Center for RNA-Seq analysis. Briefly, RNA Libraries were constructed using 500 ng of Total RNA with the TruSeq mRNA-Seq Library Construction Kit (Illumina). Libraries were quantitated with the Agilent TapeStation and the Qubit fluorometer (Thermo Fisher Scientific). qPCR was used to determine cluster density and libraries were pooled and loaded on the model no. HiSeq4000 (Illumina) using paired-end 2 × 150 cycle sequencing. Raw data were then analyzed at the National Renewable Energy Laboratory as follows. Paired-end 150-bp Illumina-read RNA-Seq data were received in the form of compressed "FASTQ" files. Samples composed of CC-124 and *fdx5* strains were harvested at four different time points of S deprivation, $t = 0, 24, 48,$ and 72 h, with three independent biological replicates for each. Thus, a total of 24 samples was analyzed. Each of the 24 samples was quality-trimmed on each end to a Q score of 20, poly-A tail-trimmed, and overlapped when possible. Read counts were performed using the pseudo-aligner "Salmon" (<https://combine-lab.github.io/salmon>) against the most current available *Chlamydomonas* transcriptome assembly 281_v5.5 (<https://genome.jgi.doe.gov/portal/>; Patro et al., 2017). Read counts were formatted into a tab-separated file and migrated to "R2" to perform differential expression using the software package "edgeR" (Robinson et al., 2010; R Core Team, 2017).

Because of the multifactor experiment design, comparison groups were assigned to each group of samples and all samples were analyzed as part of the same experiment. Low-level transcripts were filtered and removed, and all libraries were normalized to each other. Transcript counts were fit to a generalized linear model and the Cox-Reid profile-adjusted likelihood method was used to estimate the dispersion of each transcript. Differential expression was performed by a quasi-likelihood test between each condition. Differentially expressed transcripts were considered statistically significant when the corrected P value (also known as Q value, or False Discovery Rate) was ≤ 0.05 after applying a Benjamini-Hochberg correction for multiple hypothesis testing. Transcripts identified as statistically significant or noteworthy for their function were then visualized in the "Pathway Tools" browser (Karp et al., 2016), available from the BioCyc database collection (<https://biocyc.org/>).

Metabolomics Analysis

Intracellular metabolomics analysis was performed at the University of Colorado School of Medicine Metabolomics Core Facility. Three independent biological replicates were used for each time point, except for $t = 0$, which had two biological replicates. Briefly, frozen cells pellets were thawed on ice and extracted with a mixture of ice-cold methanol, acetonitrile, and water (5:3:2, respectively) at a ratio of 1 mL of extraction buffer to 5 mL of algae culture (normalized to a chlorophyll concentration of 20 μg/mL). The resulting solution was vortexed briefly to disrupt the pellet, then subjected to cold water bath sonication (30-s on/off cycles, 10 intervals) as described in Subramanian et al. (2014). Next, 0.5 mL of homogenate was transferred to a cold 1.7-mL microcentrifuge tube and centrifuged at 12,000g for 10 min at 4°C to remove insoluble materials. Supernatants were diluted 1:1 with cold extraction buffer and centrifuged again at 12,000g for 10 min at 4°C. The clarified extraction supernatants were analyzed by ultra-high pressure liquid chromatography coupled online to MS (UHPLC-MS) using a Thermo Vanquish UHPLC coupled to a Thermo Q Exactive MS. Samples were randomized and run in positive- and negative ion modes (separate runs) with an injection volume of 10 μL. UHPLC phases were water (A) and acetonitrile (B) supplemented with 0.1% formic acid for positive mode runs and 1 mM of ammonium acetate for negative mode runs. Metabolites were separated on a Kinetex C18 column (2.1 × 150 mm, 1.7 μm; Phenomenex) equipped with a guard column using a 5-min gradient method with the following conditions: flow rate = 0.45 mL/min; column temperature = 45°C; sample compartment temperature = 7°C; solvent gradient: 0–0.5 min 5% B, 0.5–1.1 min 5% to 95% B, 1.1–2.75 min hold at 95% B, 2.75–3 min 95% to 5% B,

and 3–5 min hold at 5% B. The mass spectrometer was operated in full MS mode with the following parameters: resolution = 70,000, scan range = 65–975 m/z , maximum injection time = 200 ms, microscans = 2, automatic gain control = 3×10^6 ions, electrospray source voltage = 4.0 kV, capillary temperature = 320°C, and sheath gas = 45, auxiliary gas = 15, and sweep gas = 0 (all nitrogen, in arbitrary units). Raw data files were converted to “mzXML” format using “RawConverter” (<http://fields.scripps.edu/rawconv/>) and analyzed using the software “Maven” (Princeton University) interfaced with the Kyoto Encyclopedia of Genes and Genomes database (<https://www.genome.jp/kegg/pathway.html>). Instrument stability and quality control was assessed using replicate injections of a technical mixture every 15 runs as described in Nemkov et al. (2015, 2017).

Pull-Down Assays

Pull-down assays were carried out as detailed in Peden et al. (2013). Briefly, FDX5 was covalently coupled to cyanogen bromide-activated beads (GE Healthcare) at a concentration of 5 mg per mL of resin according to the manufacturer’s instructions. To maintain the anaerobic conditions, protein extractions and pull-down experiments were carried out in a Coy chamber. Cell pellets were resuspended in 10 mL of ACA buffer (50 mM of α -aminocaproic acid, 50 mM of BisTris/HCL at pH 7.0, 0.5 mM of EDTA, and protease inhibitor), subjected to cell breakage in a cell disruptor (Aero Magics), and adjusted to a volume of 15 mL with ACA buffer. After equilibration and prereduction of 200 μ L of ferredoxin-coupled beads with 1 mM of sodium dithionite, they were incubated with 1.5-mL cell extracts on ice for 1 h. As negative controls, beads with no coupled protein, but otherwise treated the same, were also incubated with the cell extracts. The beads were then washed (25 mM of Tris at pH 7.5, 50 mM of NaCl, and 2 mM of EDTA) until the flow-through was clear and captured proteins were eluted with 200 μ L of elution buffer containing 50 mM of Tris at pH 6.8, 50 mM of dithiothreitol, and 1% (w/v) SDS. After quantification, the protein samples were subjected to trypsin digestion and analyzed by reverse-phase chromatography coupled online to an LTQ/Orbitrap MS (Thermo Fisher Scientific) as described in Peden et al. (2013).

Accession Numbers

Sequence data from this article can be found in the GenBank/EMBL data libraries under accession numbers provided in Supplemental Table S5.

Supplemental Data

The following supplemental materials are available.

Supplemental Figure S1. Relative quantification of *fdx5* transcripts by RT-qPCR in *fdx5* in comparison to the wild-type strain.

Supplemental Figure S2. Visualizations of transcriptomic differences between CC-124 wild-type and strain *fdx5* focused on photosynthesis and H₂ production pathways.

Supplemental Figure S3. Visualizations of transcriptomic differences between CC-124 wild-type and strain *fdx5* focused on Calvin–Benson–Bassham cycle.

Supplemental Figure S4. Visualizations of transcriptomic differences between CC-124 wild-type and strain *fdx5* focused on starch synthesis pathway.

Supplemental Figure S5. Visualizations of transcriptomic differences between CC-124 wild-type and strain *fdx5* focused on glycolysis pathway.

Supplemental Figure S6. Visualizations of transcriptomic differences between CC-124 wild-type and strain *fdx5* focused on tricarboxylic acid cycle

Supplemental Figure S7. Visualizations of transcriptomic differences between CC-124 wild-type and strain *fdx5* focused on acetyl-CoA synthesis pathway.

Supplemental Figure S8. Visualizations of transcriptomic differences between CC-124 wild-type and strain *fdx5* focused on fermentative pathways for the production of acetate, H₂, lactate, and ethanol.

Supplemental Table S1. Primers used in the study.

Supplemental Table S2. Global transcriptomics data.

Supplemental Table S3. Fold change of metabolites during the course of sulfur deprivation.

Supplemental Table S4. Pull-down assay results.

Supplemental Table S5. Gene accession numbers.

ACKNOWLEDGMENTS

The authors thank Chris Urban for providing laboratory support for the group. The views expressed in the article do not necessarily represent the views of the DOE or the U.S. Government. The U.S. Government retains and the publisher, by accepting the article for publication, acknowledges that the U.S. Government retains a nonexclusive, paid-up, irrevocable, worldwide license to publish or reproduce the published form of this work, or allow others to do so, for U.S. Government purposes.

Received May 3, 2019; accepted June 23, 2019; published July 26, 2019.

LITERATURE CITED

- Alizadeh D, Cohen A (2010) Red light and calmodulin regulate the expression of the *psbA* binding protein genes in *Chlamydomonas reinhardtii*. *Plant Cell Physiol* **51**: 312–322
- Boehm M, Alahuhta M, Mulder DW, Peden EA, Long H, Brunecky R, Lunin VV, King PW, Ghirardi ML, Dubini A (2016) Crystal structure and biochemical characterization of *Chlamydomonas* FDX2 reveal two residues that, when mutated, partially confer FDX2 the redox potential and catalytic properties of FDX1. *Photosynth Res* **128**: 45–57
- Buchanan BB (2016) The path to thioredoxin and redox regulation in chloroplasts. *Annu Rev Plant Biol* **67**: 1–24
- Cassier-Chauvat C, Chauvat F (2014) Function and regulation of ferredoxins in the cyanobacterium, *Synechocystis* PCC6803: Recent advances. *Life (Basel)* **4**: 666–680
- Dubini A, Mus F, Seibert M, Grossman AR, Posewitz MC (2009) Flexibility in anaerobic metabolism as revealed in a mutant of *Chlamydomonas reinhardtii* lacking hydrogenase activity. *J Biol Chem* **284**: 7201–7213
- Ghirardi ML, Subramanian V, Wecker MSA, Smolinski SL, Antonio RV, Xiong W, Gonzalez-Ballester D, Dubini A (2018) Survey of the anaerobic metabolism of various laboratory wild-type *Chlamydomonas reinhardtii* strains. *Algal Res* **35**: 355–361
- Glaring MA, Skryhan K, Kötting O, Zeeman SC, Blennow A (2012) Comprehensive survey of redox sensitive starch metabolising enzymes in *Arabidopsis thaliana*. *Plant Physiol Biochem* **58**: 89–97
- González-Ballester D, Casero D, Cokus S, Pellegrini M, Merchant SS, Grossman AR (2010) RNA-seq analysis of sulfur-deprived *Chlamydomonas* cells reveals aspects of acclimation critical for cell survival. *Plant Cell* **22**: 2058–2084
- Huang LF, Lin JY, Pan KY, Huang CK, Chu YK (2015) Overexpressing ferredoxins in *Chlamydomonas reinhardtii* increase starch and oil yields and enhance electric power production in a photo microbial fuel cell. *Int J Mol Sci* **16**: 19308–19325
- Jacobs J, Pudollek S, Hemschemeier A, Happe T (2009) A novel, anaerobically induced ferredoxin in *Chlamydomonas reinhardtii*. *FEBS Lett* **583**: 325–329
- Johnson X, Alric J (2013) Central carbon metabolism and electron transport in *Chlamydomonas reinhardtii*: Metabolic constraints for carbon partitioning between oil and starch. *Eukaryot Cell* **12**: 776–793
- Karp PD, Latendresse M, Paley SM, Krummenacker M, Ong QD, Billington R, Kothari A, Weaver D, Lee T, Subhraveti P, et al (2016) Pathway Tools version 19.0 update: Software for pathway/genome informatics and systems biology. *Brief Bioinform* **17**: 877–890
- Kosourov S, Tsygankov A, Seibert M, Ghirardi ML (2002) Sustained hydrogen photoproduction by *Chlamydomonas reinhardtii*: Effects of culture parameters. *Biotechnol Bioeng* **78**: 731–740
- Kosourov S, Seibert M, Ghirardi ML (2003) Effects of extracellular pH on the metabolic pathways in sulfur-deprived, H₂-producing *Chlamydomonas reinhardtii* cultures. *Plant Cell Physiol* **44**: 146–155
- Lambertz C, Hemschemeier A, Happe T (2010) Anaerobic expression of the ferredoxin-encoding *FDX5* gene of *Chlamydomonas reinhardtii* is regulated by the *Crr1* transcription factor. *Eukaryot Cell* **9**: 1747–1754

- Lemaire SD, Guillon B, Le Maréchal P, Keryer E, Miginiac-Maslow M, Decottignies P (2004) New thioredoxin targets in the unicellular photosynthetic eukaryote *Chlamydomonas reinhardtii*. *Proc Natl Acad Sci USA* **101**: 7475–7480
- Magneschi L, Catalanotti C, Subramanian V, Dubini A, Yang W, Mus F, Posewitz MC, Seibert M, Perata P, Grossman AR (2012) A mutant in the ADH1 gene of *Chlamydomonas reinhardtii* elicits metabolic restructuring during anaerobiosis. *Plant Physiol* **158**: 1293–1305
- Melis A, Zhang L, Forestier M, Ghirardi ML, Seibert M (2000) Sustained photobiological hydrogen gas production upon reversible inactivation of oxygen evolution in the green alga *Chlamydomonas reinhardtii*. *Plant Physiol* **122**: 127–136
- Michalska J, Zauber H, Buchanan BB, Cejudo FJ, Geigenberger P (2009) NTRC links built-in thioredoxin to light and sucrose in regulating starch synthesis in chloroplasts and amyloplasts. *Proc Natl Acad Sci USA* **106**: 9908–9913
- Nemkov T, D'Alessandro A, Hansen KC (2015) Three-minute method for amino acid analysis by UHPLC and high-resolution quadrupole orbitrap mass spectrometry. *Amino Acids* **47**: 2345–2357
- Nemkov T, Hansen KC, D'Alessandro A (2017) A three-minute method for high-throughput quantitative metabolomics and quantitative tracing experiments of central carbon and nitrogen pathways. *Rapid Commun Mass Spectrom* **31**: 663–673
- Nguyen AV, Thomas-Hall SR, Malnoë A, Timmins M, Mussgnug JH, Rupprecht J, Kruse O, Hankamer B, Schenk PM (2008) Transcriptome for photobiological hydrogen production induced by sulfur deprivation in the green alga *Chlamydomonas reinhardtii*. *Eukaryot Cell* **7**: 1965–1979
- Patro R, Duggal G, Love MI, Irizarry RA, Kingsford C (2017) Salmon provides fast and bias-aware quantification of transcript expression. *Nat Methods* **14**: 417–419
- Peden EA, Boehm M, Mulder DW, Davis R, Old WM, King PW, Ghirardi ML, Dubini A (2013) Identification of global ferredoxin interaction networks in *Chlamydomonas reinhardtii*. *J Biol Chem* **288**: 35192–35209
- Posewitz MC, Smolinski SL, Kanakagiri S, Melis A, Seibert M, Ghirardi ML (2004) Hydrogen photoproduction is attenuated by disruption of an isoamylase gene in *Chlamydomonas reinhardtii*. *Plant Cell* **16**: 2151–2163
- R Core Team (2017) R: A Language And Environment For Statistical Computing. Vienna, Austria
- Robinson MD, McCarthy DJ, Smyth GK (2010) edgeR: A Bioconductor package for differential expression analysis of digital gene expression data. *Bioinformatics* **26**: 139–140
- Sawada M, Mitsui Y, Sugiya H, Furuyama S (2000) Ribose 1,5-bisphosphate is a putative regulator of fructose 6-phosphate/fructose 1,6-bisphosphate cycle in liver. *Int J Biochem Cell Biol* **32**: 447–454
- Subramanian V, Dubini A, Astling DP, Laurens LM, Old WM, Grossman AR, Posewitz MC, Seibert M (2014) Profiling *Chlamydomonas* metabolism under dark, anoxic H₂-producing conditions using a combined proteomic, transcriptomic, and metabolomic approach. *J Proteome Res* **13**: 5431–5451
- Subramanian V, Dubini A, Ghirardi ML (2018) The role of *Chlamydomonas* ferredoxins in hydrogen production and other related metabolic functions. In *Microalgal Hydrogen Production: Achievements and Perspectives*, M Seibert, G Torzillo, eds. Royal Society of Chemistry, London, pp 213–233
- Terauchi AM, Lu SF, Zaffagnini M, Tappa S, Hirasawa M, Tripathy JN, Knaff DB, Farmer PJ, Lemaire SD, Hase T, et al (2009) Pattern of expression and substrate specificity of chloroplast ferredoxins from *Chlamydomonas reinhardtii*. *J Biol Chem* **284**: 25867–25878
- Toepel J, Illmer-Kephalides M, Jaenicke S, Straube J, May P, Goesmann A, Kruse O (2013) New insights into *Chlamydomonas reinhardtii* hydrogen production processes by combined microarray/RNA-seq transcriptomics. *Plant Biotechnol J* **11**: 717–733
- Tsygankov A, Kosourov S, Seibert M, Ghirardi ML (2002) Hydrogen photoproduction under continuous illumination by sulfur-deprived, synchronous *Chlamydomonas reinhardtii* cultures. *Int J Hydrogen Energy* **27**: 1239–1244
- Yacoby I, Pochekailov S, Toporik H, Ghirardi ML, King PW, Zhang S (2011) Photosynthetic electron partitioning between [FeFe]-hydrogenase and ferredoxin:NADP⁺-oxidoreductase (FNR) enzymes in vitro. *Proc Natl Acad Sci USA* **108**: 9396–9401
- Yang W, Wittkopp TM, Li X, Warakanont J, Dubini A, Catalanotti C, Kim RG, Nowack EC, Mackinder LC, Aksoy M, et al (2015) Critical role of *Chlamydomonas reinhardtii* ferredoxin-5 in maintaining membrane structure and dark metabolism. *Proc Natl Acad Sci USA* **112**: 14978–14983
- Yohn CB, Cohen A, Rosch C, Kuchka MR, Mayfield SP (1998) Translation of the chloroplast psbA mRNA requires the nuclear-encoded poly(A)-binding protein, RB47. *J Cell Biol* **142**: 435–442
- Zalutskaya Z, Minaeva E, Filina V, Ostroukhova M, Ermilova E (2018) Regulation of sulfur deprivation-induced expression of the ferredoxin-encoding *FDX5* gene *Chlamydomonas reinhardtii* in aerobic conditions. *Plant Physiol Biochem* **123**: 18–23